Optics & Laser Technology 169 (2024) 110111

Contents lists available at ScienceDirect

Optics and Laser Technology

journal homepage: www.elsevier.com/locate/optlastec

Full length article

Image plane digital holography for simultaneous measurement of temporal and spatial coherence

Julia Lobera, Francisco J. Torcal-Milla, Eva Mª Roche, Nieves Andres, Ana Mª Lopez, Virginia Palero, Mª Pilar Arroyo

Instituto de Investigación en Ingeniería de Aragón (I3A), Universidad de Zaragoza, 50009 Zaragoza, Spain

ARTICLE INFO

Keywords:
(090.1995) Digital holography
(120.2880) Holographic interferometry
(030.1640) Coherence
(120.3940) Metrology

ABSTRACT

In this work, we propose and validate the Image Plane Digital Holography (IPDH) with laminar illumination technique for measuring the complete coherence degree, the temporal coherence length and the spatial coherence area (transversal coherence radius), of a light source at the same time and from a single measurement. This holographic technique has been used before as a fluid velocimetry technique that allows measuring the three components of the fluid velocity in a plane. Since its performance is limited by the temporal and spatial coherence of the laser, we can take advantage of this and make IPDH with laminar illumination a means of obtaining these laser properties. The proposed method could be of interest for the optics community since it could be used for any type of light source, presenting some advantages by comparing it with other well-established techniques. It has been tested by using a high repetition rate laser commonly used in velocimetry and the results have been compared to those obtained with other standard techniques, verifying the well-functioning of the IPDH-based technique.

1. Introduction

The coherence degree of a light source is related to the ability of the source to produce interferences [1,2]. This magnitude is commonly obtained by using interferometric set-ups. Temporal coherence gives a measurement of the maximum delay between two identical waves that come from the same point of the source, which are able to produce interferences. On the other hand, spatial coherence gives a measurement of the maximum transversal distance between two different points of a wavefront which are able to interfere, i. e. the radius of the spatial coherent area. Spatial and temporal coherence are usually measured with separated experimental configurations. Temporal coherence can be measured with Michelson interferometers [3–5], modified Mach-Zehnder interferometers [6], among other more sophisticated techniques [7,8], and spatial coherence is usually measured with several realizations of the classical Young's experiment, lateral shearing interferometry, or modified Mach-Zehnder interferometers [9–14]. However, the measurement of the spatial coherence with a double pin-hole experiment disregards the simultaneous effect of the temporal coherence on the coherence degree. In this work, we propose to use a holographic set-up to obtain the temporal and spatial coherence degree of a light source simultaneously from a single measurement. The proposed technique is called Image Plane Digital Holography (IPDH) with laminar illumination [15–17], which is an off-axis holographic technique that has shown its applicability for the measurement of the whole velocity field in a fluid plane [18] and for particle sizing [19,20]. When IPDH is applied in fluid velocimetry, the flow is seeded with particles that are illuminated with a very narrow laminar beam. The fluid plane is imaged onto a digital camera as in Particle Image Velocimetry (PIV) and interferes at the camera sensor with an off-axis reference beam, making a so-called image hologram. The region where both beams interfere is limited by the laser coherence degree and this restriction can be used to measure the coherence degree of the laser and therefore, the spatial and temporal coherence lengths simultaneously. A double cavity high repetition rate laser is used in this work as light source to test the technique, although it could be applied to any other light sources. The main features of a high repetition rate laser are its out-put energy and its repetition rate, meanwhile its spectral bandwidth and its coherence properties usually remain unknown. In our work, the interference term of the hologram obtained by means of IPDH-based optical set-up provides useful information of the laser optical coherence properties that will be detailed in next sections. As we will show, the horizontal width of the coherent region of the hologram at the camera plane can be related with the laser temporal coherence length and its vertical width, with the

E-mail address: fjtorcal@unizar.es (F.J. Torcal-Milla).

https://doi.org/10.1016/j.optlastec.2023.110111
Received 30 March 2023; Received in revised form 8 September 2023; Accepted 18 September 2023
Available online 25 September 2023

spatial coherence radius, giving a simultaneous measurement of both. Other holography-based techniques have been proposed to measure the temporal coherence of pulsed laser sources [21,22], but in our proposal, complete coherence information of the laser can be obtained from a single measurement with the same set-up. In the following sections, we describe the most relevant IPDH characteristics that are useful for our purpose. Then, we explain how we can use them to measure the temporal coherence length and the spatial coherence radius of a light source, such as a double cavity high repetition rate laser, simultaneously. We discuss the obtained results along each section, compare them with those obtained with other standard techniques, and highlight the main conclusions at the end of the manuscript.

2. Image plane digital holography

The proposed set-up consists of a common IPDH set-up in which a wedge divides the laser beam in two beams, which are redirected by the mirrors within two commercial optical guiding arms (Fig. 1a). The strongest beam (illumination beam) is shaped by a set of spherical lenses, which focus the beam in the center of the object, and a cylindrical lens that expands the beam along the vertical direction. Thus, the beam results very slim in one transversal direction and elongated in the other one. Then, the illumination beam passes through the object along its length and the laterally scattered light is used as object beam. An objective is used to image the object at a plane near the camera sensor. In the other beam (reference beam), a lens is used to produce a divergent wave, whose source would be located at the same distance from the sensor as the objective aperture. Thus, this holographic set-up can be also considered as a lensless Fourier transform hologram of the lens aperture [16]. This interpretation has the advantage of allowing an easy isolation of the real image from the virtual image in the Fourier domain of the reconstructed hologram, as it will be explained along this section. This fact results crucial for the performance of the technique.

The laser beam can be considered to originate from an extended light source since it has an appreciable diameter (1.5 mm), and the expansion rate and orientation of both the reference and the object beams (as seen at the camera sensor) have to be well controlled in order to spatially match the corresponding points and ensure they are spatially coherent. Since the laser is linearly polarized, we used the polarization direction to orientate both beams. The articulated parts of the two guiding arms were arranged so that both beams were vertically polarized (Y-axis in Fig. 1a).

The intensity recorded by the camera provides information about the mutual coherence function, defined as [1]

$$\Gamma(\vec{s}_1, \vec{s}_2, \tau) = \left\langle \tilde{E}(\vec{s}_1, t+\tau)\tilde{E}^*(\vec{s}_2, t) \right\rangle, \tag{1}$$

where $\vec{s}_1$ and $\vec{s}_2$ are two points of the hologram, t is the time, τ is the delay between both beams, $\tilde{E}\left(\vec{s}_1, t+\tau\right) = \tilde{r}$ is the reference beam (Fig. 1b), $\tilde{E}\left(\vec{s}_2, t\right) = \tilde{o}$ is the object beam (Fig. 1c), and * denotes complex conjugated. Let us note that these images and all the 2D black and white images along the whole paper are shown rescaled such that the 5% brightest points were set to the maximum grey level (255) in order to enhance the relevant spatial information.

For coherence issues, the important magnitude is the complex degree of coherence, defined as

$$\gamma(\vec{s}_1, \vec{s}_2, \tau) = \frac{\Gamma(\vec{s}_1, \vec{s}_2, \tau)}{|\tilde{r}||\tilde{o}|}. \tag{2}$$

According to the definitions made after Eq. (1), at each point of the hologram, $\tilde{r}$ comes from a certain point of the source, $\vec{s}_1$, and $\tilde{o}$ from another point of the source, $\vec{s}_2$, with a time delay between them $\tau = OPD/c$, where OPD is the optical path length difference between $\tilde{o}$, and $\tilde{r}$, and c is the speed of light. By using Eq. (2), the intensity at the camera, i.e. the hologram intensity, can be expressed as

$$I = |\tilde{r}|^2 + |\tilde{o}|^2 + |\gamma|\tilde{r}^*\tilde{o} + |\gamma|\tilde{r}\tilde{o}^*. \tag{3}$$

Thus, the modulus of the complex degree of coherence, i.e. the degree of coherence $|\gamma|$, which depends on the temporal and spatial coherence between both beams (reference and object) at any point of the camera sensor, can be recovered from the interference terms of Eq. (3). The four terms in Eq. (3) are mixed in the spatial domain but they can be separated in the frequency domain, as usual [16–20]. The Fourier transform of the intensity recorded in the hologram can be expressed as

$$\Im\{I\} = |\tilde{r}|^2\delta(0,0) + \Im\left(|\tilde{o}|^2\right) + \Im\{|\gamma|\tilde{r}^*\tilde{o}\} + \Im\{|\gamma|\tilde{r}\tilde{o}^*\}, \tag{4}$$

where $\Im$ represents the Fourier transform. Fig. 2a shows the Fourier transform intensity of one of these holograms. The background term contains the Fourier transform of $|\tilde{o}|^2$, and $|\tilde{r}|^2$. The heptagons, which can be appreciated near the up-left and down-right corners of Fig. 2a, are the real and virtual images of the lens aperture (the third and fourth terms in Eq. (4)). With our IPDH configuration, the interference terms have only significant values on a reduced area of the hologram, where the object beam has the appropriate optical path to produce interferences with the reference beam, meanwhile all the object beam contributes to the second term $\Im\left(|\tilde{o}|^2\right)$. Thus, the intensity of the heptagons as compared to the background term seems lower. This can be illustrated more clearly by calculating the Fourier transform for each 256 × 256 pixels window of the intensity recorded in the hologram and obtaining the corresponding Fourier transform map (Fig. 2b). The presence of the real and virtual images of the lens aperture in this map indicates the regions where the reference and the object beam are interfering: the heptagons only appear in the fourth column of the resultant image, which

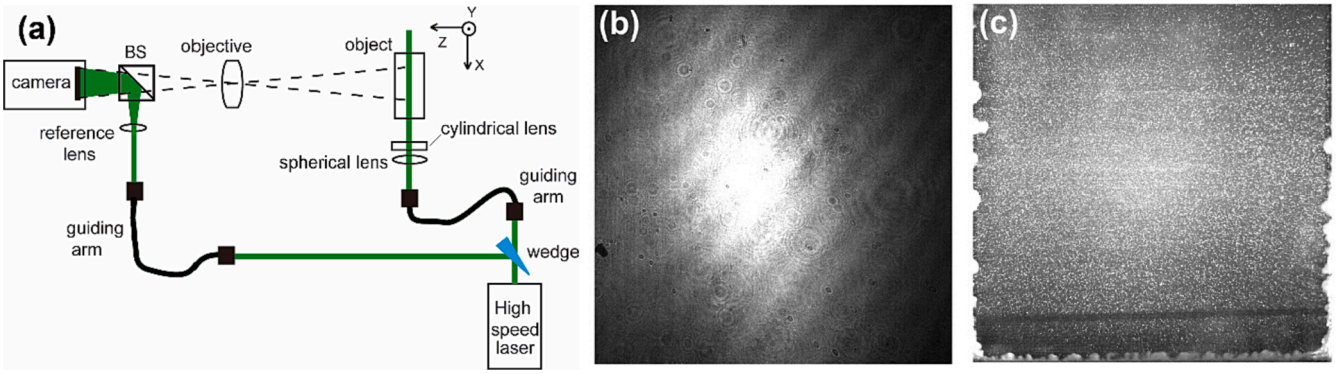

Fig. 1. (a) Schematic drawing of the experimental set-up; representative images of the (b) reference beam and (c) object beam.

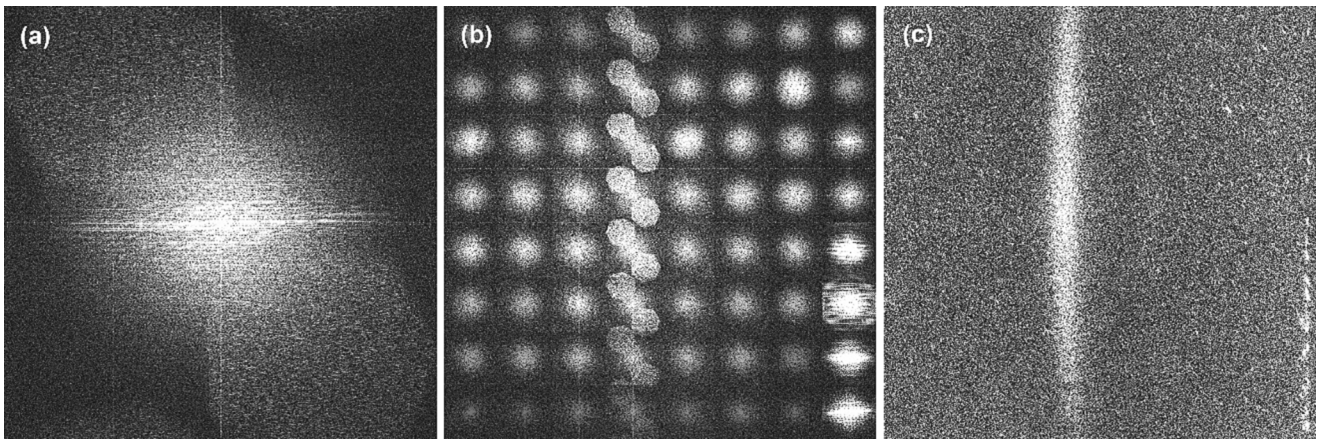

Fig. 2. Interference term of an IPDH recording: Fourier Transform of (a) the whole hologram and (b) windows with 256x256 pixel size; (c) Amplitude map in which the coherence area is clearly observed.

corresponds to the interference area. Let us note that the high intensity at the bottom of the last column is not an interference pattern, it is due to a strong reflection at the object entrance, which makes the second term of Eq. (4) clearly visible.

In the digital reconstruction of the holographic recording, the real image of the lens aperture is selected and moved to the centre of the Fourier plane, while the rest is blocked [16–20]. Then, the inverse Fourier transform is computed so the complex amplitude distribution, $|\gamma|\widetilde{r}^{*}\widetilde{o}$, at the object plane is recovered. The modulus of this function depends not only on the degree of coherence but also on $\widetilde{r}$ and $\widetilde{o}$. Since our reference beam is smoothly variable although not completely uniform, it is convenient to remove $\widetilde{r}$ from the reconstructed field by dividing by it. Thus, we have recorded the reference beam intensity, Fig. 1b, and obtained $|\widetilde{r}|$ by using a similar procedure as the used to isolate the interference term in the Fourier transformed hologram.

On the other hand, the object beam has a speckle structure and, therefore, it is more adequate to remove its influence by a statistical approach, as it will be explained along the next sections. Fig. 2c presents the resulting amplitude, $a = |\gamma||\widetilde{o}|$, obtained from one hologram after performing the Fourier transform operations and dividing it by the reference beam, showing a vertical bright fringe, which is the region where the reference and the object beams interfere at the sensor plane. The object beam $\widetilde{o}$ is not a faithful copy of $\widetilde{r}$ and those differences determine the dimensions of the coherent region. The reference beam at the camera sensor is a measurement of the laser intensity profile but magnified from the initial size of the laser beam with a magnification factor, M_r. On the other side, the object beam is compressed along the optical axis (Z-axis in Fig. 1a) and reaches the sensor with a different vertical magnification factor, M_o. Thus, we need to adjust the optics to ensure that both beams overlap very well along the vertical direction (Y-axis in Fig. 1a). On the contrary, the adjustment along the horizontal direction is not so critical since there is always some part of the so-called object beam that is spatially coherent with the reference beam.

The object beam optical path increases as it travels through the object (X-axis in Fig. 1a). Therefore, the horizontal width of the coherent region is limited by the temporal coherence of the source and its vertical width is limited by the spatial coherence of the source. These facts will be used to obtain the coherence properties of the beam, as it will be detailed in the next sections.

3. Temporal coherence length measurement

Assuming that the spatial coherence is optimized, the maximum degree of coherence is obtained when the optical path length difference between both beams (*OPD*) is null. To achieve this, the optical path lengths for both the object and the reference beams have to be matched within the temporal coherence length of the source at a chosen point at the camera sensor. Fig. 2c shows the coherent area whose central vertical line has null *OPD* between the reference and the object beams. This central line has a slight curvature due to the different optical path length for each light ray going from the object to its corresponding point at the camera sensor (image plane). The *OPD* increases as the illuminating beam travels along the object, i.e. as we move towards the left of the image. The dependence of the coherence degree on the *OPD* can be studied by analyzing the changes in the amplitude of the reconstructed filtered hologram along the X-axis.

In our specific set-up, a double cavity New Wave Pegasus high repetition rate laser ($\lambda = 527\ nm$, energy per pulse = 10 mJ at 1000 Hz, pulse width $\leqslant$ 180 ns) is used as light source and the object consists of a transparent solid object made of polymethyl methacrylate (PMMA, refractive index, $n_{PMMA} = 1.492$) seeded with particles that scatter the illumination beam. Finally, a high-speed CMOS camera (Fastcam SA2, 16 bits, 2048x2048, pixel size of 10 μm × 10 μm, 1000 fps) and a photographic objective ($f' = 105\ mm$) are used to record the hologram plane with a magnification of $M = 0.411$.

Fig. 3a-b present a vertically centered 500px-wide, 150px-high region of the amplitude map (as in Fig. 2c) obtained for our two laser cavities, A and B. The temporal coherence length, L_c, can be estimated as the width of the interference area along the X-axis, since two particles horizontally displaced into the object receive and scatter the light with a certain delay. As it can be observed, a lot of speckle appears and therefore, the width of the coherent area, i. e. the temporal coherence length, is better determined from the vertically averaged coherence degree. Fig. 3c shows the coherence degree as computed from the experiments of Fig. 3 a) (blue line) and b) (red line). The temporal coherence length is directly related with the width of the graphs at *1/e* of the maximum (black solid line in Fig. 3c) by adjusting the data to a Gaussian function after subtracting the background, as usual. From Fig. 3c it can be also deduced that the temporal coherence length for the cavity B is 25% bigger than for the cavity A.

The temporal coherence length in air, L_c, is obtained from the measured width of the Gaussian fitting, Δx, by taking into account the pixel size of the camera, px, the magnification of the imaging system, M, and the object refractive index, n, such as $L_c = px\Delta xn/M$, which allows giving a quantitative value of the temporal coherence length of the source, (Table 1). We have also included the estimated errors from the Gaussian fitting considering a confidence interval of 95%. However, we have experimentally checked that, when IPDH is used as a velocimetry technique, the size of the useful region of the hologram can be defined with a less restrictive criterion than for the temporal coherence length, L_c, since the used length requires a SNR much smaller. For that reason, we have also computed the width of the region with a coherence degree

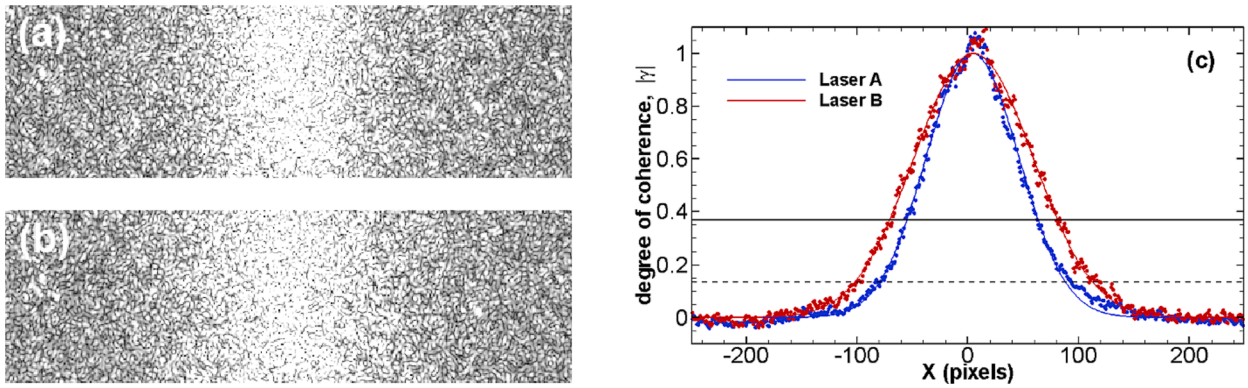

Fig. 3. Region of the computed amplitude for (a) cavity A, (b) cavity B, and (c) modulus of the coherence degree along the X-axis obtained for both laser cavities.

Table 1
Temporal coherence length computed for both cavities of the laser with the proposed method.

Laser cavity	Δx(px)	L_c (mm)	L_u (mm)
A	119.8 ± 1.7	4.35 ± 0.06	6.15 ± 0.08
B	151.8 ± 2.5	5.51 ± 0.09	7.85 ± 0.13

bigger than $1/e^2$ of the maximum (dashed line in Fig. 3c), and the corresponding useful coherence length, L_u, (Table 1). To check the validity of the obtained results, we have measured the temporal coherence length with a modified interferometer similar to that shown in [23], obtaining $L_{c,A} = 4.98 \pm 0.15\ mm$, and $L_{c,B} = 5.33 \pm 0.17\ mm$. These results are in agreement with our present values and corroborates that laser cavity B has a temporal coherence length larger than laser cavity A.

4. Spatial coherence radius measurement

Since the spatial coherence area of a beam increases with the distance from the light source, we have chosen a specific plane, far from the laser output, and close to our working region to obtain its transversal spatial coherence radius (radius of the spatially coherent area). Fig. 4 shows the beam profiles for both laser cavities at this plane, which is just before the reference lens plane, at a distance $d_L = 3.256\ m$ from the wedge, Fig. 1a. It can be seen that both cavities have elongated intensity profiles but with different shapes.

As we have mentioned, the spatial coherence radius is related to the vertical (Y-axis) width of the envelope of the interference term of the hologram, since two particles vertically displaced into the object receive the light from the source at the same time. Thus, the scattered light from these two particles would be fully temporally coherent, being the whole coherence effect due to the spatial coherence. As in any interferometric recording, a good spatial coherence requires both beams to have the same orientation, similar size and very good overlapping. In an IPDH configuration, it implies to control the vertical alignment and to have similar values for the magnification factor of both beams, M_r and M_o. In an ideal case, at any point at the camera sensor, the object and the reference beams should come from the same point of the laser beam but, in a more general case, they come from two very close points $\vec{s}_1$ and $\vec{s}_2$. The distance, h, in the vertical direction, between $\vec{s}_1$ and $\vec{s}_2$ can be expressed as a function of the magnification factors of the object beam, M_o, and the reference beam, M_r, with respect to the chosen plane at d_L

$$h = (y - y_0)\left(\frac{1}{M_o} - \frac{1}{M_r}\right), \tag{5}$$

where y is the vertical coordinate at the sensor plane and y_0 is a constant, which depends on the vertical beam alignment.

If the magnifications are very similar, h is approximately constant along the Y-axis of the recorded region and it is not possible to extract information about the spatial coherence from the hologram. Therefore, we need that $M_o \neq M_r$. Besides, if one of the beams is flipped in the vertical direction, then

$$h = (y - y_0)\left(\frac{1}{M_o} + \frac{1}{M_r}\right). \tag{6}$$

Thus, h changes notably along the Y-axis, and the alignment of the beams is irrelevant since it only determines where the radius h is null, i.e. where the center of the interference region is located. Moreover, if the *OPD* is null, with a vertically flipped reference beam, there is always a region of coherence with good contrast.

The coherence degree reaches the same value when h is either positive or negative. Subsequently, the total vertical width of the coherent

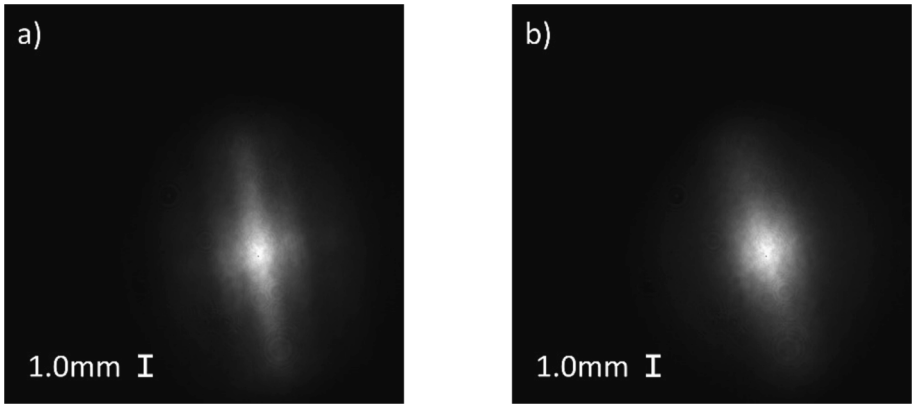

Fig. 4. Laser beam profiles at 3.256 m from the wedge at the maximum energy conditions: a) for laser cavity A and b) for laser cavity B.

region, $\Delta y = (y - y_0)$, is twice the maximum separation h between two source points spatially coherent. Then, the radius of the spatially coherent area at d_L considering both cases (Eq. (6) and Eq. (7)), can be computed as

$$\rho_c = \frac{\Delta y}{2}\left(\frac{1}{M_o} \mp \frac{1}{M_r}\right). \tag{7}$$

Thus, to obtain the spatial coherence radius, ρ_c, we need to determine the magnification factors of the reference beam, M_r, and of the object beam, M_o, and to measure the width, $\Delta y = (y - y_0)$, along the vertical direction, in a similar way as we have measured the width along the horizontal direction in the previous section.

On one hand, the object beam magnification, M_o, can be computed by taking into account the laser diameter before the lenses that produce the illumination beam of the object and the expansion produced by them, besides the magnification of the imaging lens, M. Then, the object beam magnification can be expressed as

$$M_o = \frac{d_O}{d_L}\frac{x_{ilu}}{n f_{ilu}} M, \tag{8}$$

where d_O is the distance from the wedge to the first spherical lens (see Fig. 1a), f_{ilu} is the focal length of the cylindrical lens, and x_{ilu} is the distance from the centre of the imaged object area to the origin of the illuminating beam. In our setup, $d_O = 2.478\ mm$, $f_{ilu} = -50\ mm$ and $x_{ilu} = 675\ mm$, so $M_o = 2.93$.

On the other hand, the reference beam magnification, M_r, can be computed by taking into account the laser diameter at the reference lens position, $d_r \approx d_L$, the focal length of the reference lens, f_r, and the beam expansion produced by this lens. This beam expansion can be computed by considering the reference beam as a divergent wave that comes from a distance equal to the image distance of the imaging system. Then, the reference magnification can be expressed as

$$M_r = \frac{d_r}{d_L}\frac{f(1+M)}{f_r}. \tag{9}$$

Once the theoretical formalism is established, we have considered three experimental cases: in case 1 we consider the same configuration as in Figs. 2-4, with a reference lens with $f_r = 40\ mm$ and $M_r = 3.70$; in case 2 the output arm of the reference beam is vertically flipped and the reference lens is the same as in case 1; and in case 3 the reference beam is not flipped but the focal length of the reference lens is modified, $f_r = 10\ mm$, resulting in $M_r = 14.82$. We have checked that the magnifications of the reference beam, determined from the comparison of the laser beam profile (Fig. 4) with the profiles on the sensor (Fig. 1b), and the object beam, give similar values.

Fig. 5 shows the amplitude map and its dependence on the Y-coordinate for the three considered cases. For each case, we present a 300px-wide region of the amplitude map and its horizontal average. Let us remark that the coherent region is not limited by the size of the object and reference beams, as both fill the whole region of the sensor. The object beam has not been modified from previous experiments (Fig. 1c), and there is no appreciable difference between the intensity distribution of the reference beams for case 1 and case 2. For case 3, the reference intensity distribution is even more uniform as we have expanded further the beam. In the case 1 (Fig. 5a), we can appreciate that the amplitude does not represent the full coherent region as the amplitude does not decrease to zero. In addition, as the peak is very wide, the Gaussian fit is quite sensitive to the data noise. In order to improve the spatial coherence radius measurement, we need a shorter fringe so that the amplitude changes noticeably between the centre and the extremes, where it should reach an off-set value. To achieve it, we can either rotate the reference arm output to obtain a vertically flipped reference beam (case 2, Fig. 5b), or change the magnification of one of the beams (case 3, Fig. 5c).

With a vertically flipped reference (Fig. 5b), the vertical width of the interference term is clearly reduced and we can appreciate the amplitude dependence on the Y-coordinate. A similar result is obtained when the reference lens is modified to expand further the reference beam (Fig. 5c).

We have fitted the amplitude to a Gaussian function to determine the full vertical width at $1/e$ of the maximum value as in the previous section, and the spatial coherence radius according to Eq. (7). The resultant values are presented in Table 2. We have also computed the useful distance, at which we can still have useful interference at $1/e^2$ of the maximum, which is usually enough for interferometric measurements, Table 2. In addition, we have included the estimated errors from the Gaussian fitting considering a confidence interval of 95%.

In the three cases, the variability of the data and its discrepancy with the Gaussian fit is notably bigger (Fig. 6) than in the previous section (see Fig. 3). The reason is that the interference fringe is very narrow and the average in the X-direction includes only a few speckles. The configuration used in case 1 does not provide data along h to resolve the full dependence of the coherence degree (Fig. 5a), and therefore the

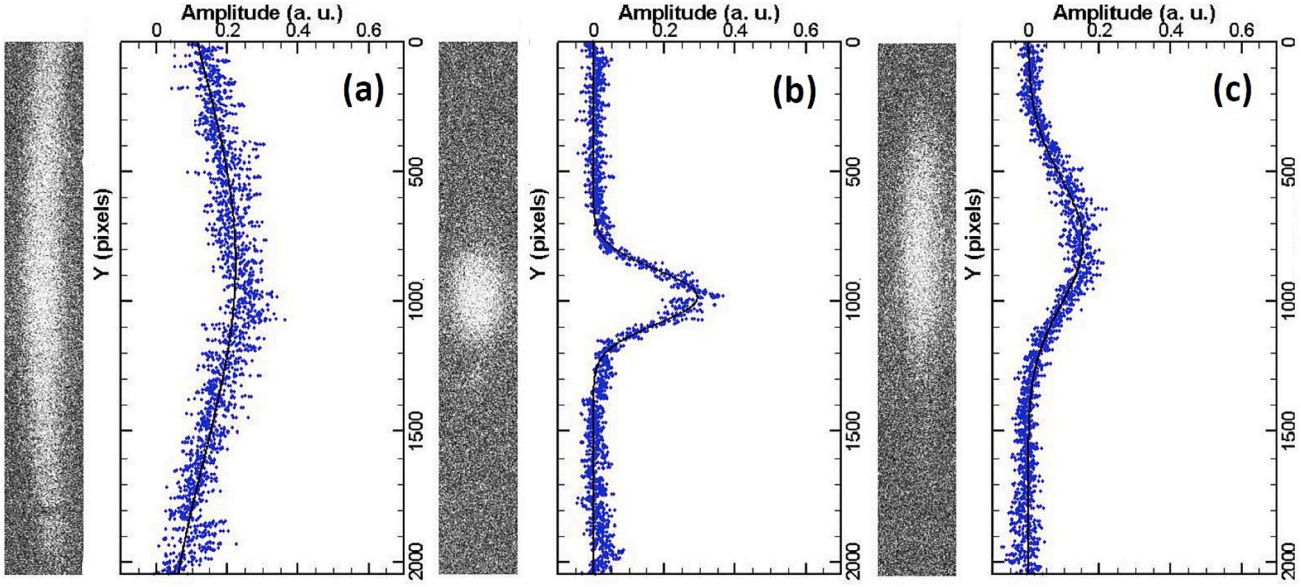

Fig. 5. Interference term and averaged amplitude along the Y-coordinate obtained for a) case 1, b) case 2, and c) case 3.

Table 2
Spatial coherence radius computed for both cavities of the laser and the three considered cases.

Case	Laser cavity	Reference output	Δy(px)	ρ_c(mm)	ρ_u(mm)
1	A	No flipped	2107.7 ± 44.6	0.756 ± 0.016	1.069 ± 0.023
	B	No flipped	1689.6 ± 28.6	0.606 ± 0.01	0.857 ± 0.01
2	A	flipped	294.1 ± 3.3	0.900 ± 0.010	1.272 ± 0.028
	B	flipped	353.1 ± 6.3	1.080 ± 0.019	1.528 ± 0.027
3	A	No flipped	685.4 ± 12.4	0.937 ± 0.017	1.326 ± 0.025
	B	No flipped	743.7 ± 13.4	1.017 ± 0.018	1.438 ± 0.026

spatial coherence radius cannot be determined accurately. This problem is solved for cases 2 and 3, which provide very similar results. The same conclusions can be deduced from the measurement of cavities A and B, being the main difference that the spatial coherence radius is bigger for the laser cavity B than for the cavity A. The spatial coherence radius can be related with the size of the laser profile near the reference lens (Fig. 4). The ratio of the coherence area and the laser beam size remains constant for any other plane, as the governing equations for the mutual coherence degree propagation through free media or optical systems are the same as for the beam propagation itself [1]. However, this ratio depends on the chosen criteria for the beam diameter definition. Thus, we use the angle subtended by the coherence radius at the chosen plane, $\theta_c = 2\rho_c/d_L$, and compare it with the beam divergence given by the manufacturer, $\leq$3 mrad. The average θ_c calculated for cases 2 and 3 results 0.6 mrad. This result justifies the need to adjust the expansion rate and the orientation of both beams according to what we found in the experimental implementation of our setup. Also, we can expect a coherence degree greater than $1/e$ of the maximum when we make interfering two beams shifted less that a 20% of the beam dimensions for any of both laser cavities.

To validate these results, we performed some experiments with a modified Mach-Zehnder interferometer similar to that shown in [14], with a distance $d_L = 5\ m$. We measured that in the vertical direction, $\rho_c = 0.803 \pm 0.004\ mm$ for laser cavity A and $\rho_c = 1.038 \pm 0.004\ mm$ for laser cavity B, which give an average angle subtended by the coherence radius of 0.32 mrad and 0.42 mrad, respectively. These results are in agreement with our present values and corroborates that laser B has a coherence radius larger than laser A.

5. Conclusions

In this work, we present a complete holographic technique for measuring simultaneously the temporal coherence length and the spatial coherence radius of a light source. We take advantage of the performance dependence of a Image Plane Digital Holography set-up with laminar object illumination on the coherence properties of the illumination beam to produce interferences. The temporal coherence length is obtained from the vertical average of the envelope of the interference term of the hologram and the spatial coherence radius is computed from the horizontal average of the same envelope, both separately obtained from the complex degree of coherence. The resultant measurements are in agreement with other experiments performed with two separated set-ups. The main advantages of the presented technique are that the measurement of the spatial and temporal coherence can be computed by using the same set-up from a single recording and that the influence between them is almost unlinked. In addition, an experimental aproach to the coherence length calculations suggests that the criteria of $1/e$ of the maximum is too exigent, since for the most practical cases the used coherence length requires a SNR much smaller. Therefore, we have also defined and computed an useful coherence length at $1/e^2$ of the maximum. Finally, the presented procedure has been applied to a double cavity high repetition rate laser but it could be applied to obtain the coherence properties of any other type of illumination source.

Funding, acknowledgments, and disclosures

Spanish Ministerio de Ciencia e Innovación PID2020-113303GB-C22/AEI/10.13039/501100011033; Gobierno de Aragón - Fondo social europeo (Laser Optical Technology E44_23R research group); Universidad de Zaragoza UZ2020-CIE-04.

CRediT authorship contribution statement

Julia Lobera: Investigation, Software, Writing – original draft, Project administration. **Francisco J. Torcal-Milla:** Formal analysis, Writing – review & editing. **Eva Mª Roche:** Investigation. **Nieves Andrés:** Writing – review & editing. **Ana Lopez:** Software, Writing – review & editing. **Virginia Palero:** Writing – original draft, Project administration. **Mª Pilar Arroyo:** Conceptualization, Investigation, Writing – original draft.

Declaration of Competing Interest

The authors declare that they have no known competing financial interests or personal relationships that could have appeared to influence

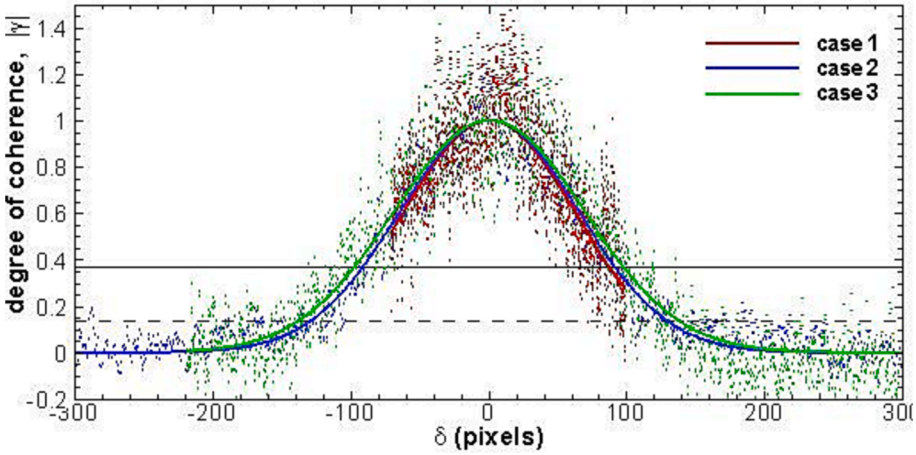

Fig. 6. Coherence degree of laser cavity A along vertical coordinate at the laser profile shown in Fig. 5a..

the work reported in this paper.

Data availability

Data will be made available on request.

References

[1] B.E.A. Saleh, M.C. Teich, Fundamental of Photonics, Chapter 10, Jonh Wiley & Sons, 2007.
[2] J. Perina, Coherence of light, Van Nostrand Reinhold Company, 1972.
[3] V.P. Ryabukho, D.V. Lyakin, V.V. Lychagov, What type of coherence of the optical field is observed in the michelson interferometer, Opt. Spectros. 102 (2007) 918–926.
[4] M. Singh, S. Datta, Dual measurements of temporal and spatial coherence of light in a single experimental setup using a modified Michelson interferometer, Rev. Sci. Instrum. 92 (2021), 105109.
[5] L.P. Leppänen, et al., Measurement of the degree of temporal coherence of unpolarized light beams, Photonic Res. 5 (2017) 156–161.
[6] F.J. Torcal-Milla, J. Lobera, A.M. Lopez, V. Palero, N. Andres, M.P. Arroyo, Mach-Zehnder-based measurement of light emitting diodes temporal coherence, Optik 267 (2022), 169722.
[7] W.A. Ramadan, H.H. Wahba, A.S. El-Tawargy, Enhanced short temporal coherence length measurement using Newton's rings interference, Opt. Laser Technol. 127 (2020), 106192.
[8] R. Dubey, R. Kumar, A simple setup for measurement of the coherence length of a laser diode using holographic optics, European J. Phys. 40 (2019) 055304 (9pp).
[9] N. Singh, H.S. Vora, On the coherence measurement of a narrow bandwidth dye laser, App. Phys. B 110 (2013) 483–489.
[10] L. Pan, et al., Measuring spatial coherence by using a lateral shearing interferometry, App. Opt. 58 (2019) 56–61.
[11] M. Santarsiero, R. Borghi, Measuring spatial coherence by using a reversed-wavefront Young interferometer, Opt. Lett. 31 (2006) 861–863.
[12] K. Saastamoinen, et al., Spatial coherence measurement of polychromatic light with modified Young's interferometer, Opt. Express 21 (2013) 4061–4071.
[13] A. Luis, Modulation of coherence of vectorial electromagnetic waves in the Young interferometer, Opt. Lett. 33 (2008) 1497–1499.
[14] F.J. Torcal-Milla, J. Lobera, E.M. Roche, A.M. Lopez, V. Palero, N. Andres, M. P. Arroyo, Modified Mach-Zehnder interferometer for spatial coherence measurement, Opt. Lett. 48 (2023) 3127–3130.
[15] U. Schnars, W. Jüptner, Digital holography, Springer, 2005.
[16] J. Lobera, J.N. Andrés, M.P. Arroyo, Digital Image Plane Holography as a three-dimensional flow velocimetry technique, Proc. SPIE 4933 (2003) 279–284.
[17] J. Lobera, J.N. Andrés, M.P. Arroyo, Digital speckle interferometry as a holographic velocimetry technique, Meas. Sci. Technol. 15 (2004) 718–724.
[18] V. Palero, J. Lobera, M.P. Arroyo, Three-component velocity field measurement in confined liquid flows with high speed digital image plane holography, Exp. Fluids 49 (2010) 471–483.
[19] V. Palero, J. Lobera, M.P. Arroyo, Digital Image Plane Holography (DIPH) for two-phase flow diagnostics in multiple planes, Exp. Fluids 39 (2005) 397–406.
[20] V. Palero, M.P. Arroyo, J. Soria, Digital holography for micro-droplet diagnostics, Exp. Fluids 43 (2007) 185–195.
[21] I.N. Ross, Design and operation of holographic techniques for measuring coherence, Opt. Acta 22 (1975) 639–651.
[22] R.F. Wuerker, J. Munch, L.O. Heflinger, Coherence length measured directly by holography, App. Opt. 28 (1989) 1015–1017.
[23] A. Halder, H. Partanen, A. Leinonen, M. Koivurova, T.K. Hakala, T. Setälä, J. Turunen, A.T. Friberg, Mirror-based scanning wavefront-folding interferometer for coherence measurements, Opt. Lett. 45 (2020) 4260–4263.